Tuning the selectivities of Mg-Al mixed oxides for ethanol upgrading reactions through the presence of transition metals

Jorge Quesada, Laura Faba, Eva Díaz and Salvador Ordóñez*

Department of Chemical and Environmental Engineering, University of Oviedo. c/ Julián Clavería, s/n, 33006, Oviedo, Spain. Email: sordonez@uniovi.es

ABSTRACT

The effect of the presence of reduced Co and Ni (chosen as representative metals because of their good activity for dehydrogenation reactions) on the catalytic performance of basic mixed oxide (Mg-Al) for ethanol condensation is studied in this work. This effect has been studied both in absence and in presence of hydrogen, and considering the different steps of this complex reaction. Globally, best results were obtained with Co/Mg-Al, under reducing atmosphere, at mild temperature (below 600 K). At these conditons, 1-butanol production rates up to eight times higher than the obtained with Mg-Al under inert atmosphere. Co has a marked activity in the dehydrogenation step, that prevails over its less relevant activity in aldolization and hydrogenation reactions. This result indicates the relevant role of this first reaction step. DRIFT spectroscopy analyses were carried out to support the experimental results and to identify the role of hydrogen and metals on the oligomerization and permanent adsorption processes, which can produce the deactivation of the catalyst.

KEYWORDS: Butanol, Cobalt, Nickel, Dehydrogenation, Hydrogenation, Aldol Condensation

1. Introduction

Gas-phase ethanol condensation has been intensively investigated in the last few years, because of the high potential of ethanol as bioplatform molecule [1-4]. Among the different chemicals obtained from ethanol [5-8], 1-butanol is the most valuable one, with better fuel properties than ethanol, and many uses as solvent and platform molecule. There is not agreement about the actual mechanism for 1-butanol formation. The so-called four-step mechanism (**Scheme 1**) is the most accepted one, although several authors also suggest the direct ethanol condensation or the acetaldehyde-ethanol reaction [4,9-11]. According to the four-step mechanism, acetaldehyde aldolization is usually considered as the rate-determining step since it involves two molecules, and different active sites, requiring an appropriate balance between acid and medium-strength basic sites. Different materials, mainly mixed oxides and hydroxyapatites (HPA) have been proposed as promising catalysts [4,11-12]. Despite their good activity for aldolization, experimental results indicate that the difficulty in activating the α-hydrogen of the ethoxides (previous ethanol dehydrogenation) strongly limits the final yields [13-15]. This effect was previously observed for the dehydrogenation of different alcohols, the use of transition metals in the reduced form (Co, Ni, Cu, Fe, Ir, etc.) being proposed for reducing the activation energy of the αC-H bond scission [16,17]. In addition, reduced metals are supposed to alter the acid/base sites distribution in a lower extent that the metal oxides.

Under inert conditions, or in absence of any active metal for the molecular hydrogen activation, once the acetaldehyde reacts producing crotonaldehyde, the 1-butanol is obtained upon two subsequent hydrogenations: terminal C=O bonds hydrogenation through the Meerwein-Ponndorf-Verley (MPV) reduction (crotonaldehyde and butanal), and hydrogenation of the unsaturated intermediates (crotonaldehyde and crotyl alcohol) by surface-mediated hydrogen transfer reaction

[6,9]. Under these conditions, ethanol molecules are the hydrogen source for the former hydrogenation [18], being the hydrogen released in the dehydrogenation step [15,18,19]. HPA and mixed oxides are not very active for these reactions, so the global process is still far to be optimized.

This work is focused on the study of the effect of supporting transition metals and including hydrogen in the feed on the performance of Mg-Al mixed oxides for ethanol gas-phase condensation. It was previously suggested that the use of reducing conditions, in addition to the expected improvement in hydrogenation steps, has a positive effect on the catalyst stability, preventing the permanent deposition of unsaturated molecules [20]. Mg-Al mixed oxide was chosen as bulk material, considering the well-known behaviour of this material for this reaction [6]. The idea of using metal-modified oxides has been previously proposed by some authors, studying the effect on the upgrading of different alcohols, such as methanol or ethanol [21-23]. In this context, Co and Ni are good candidates because of their high activity for alcohol dehydrogenations [23,24]. However, most of the reported studies are performed with very high metal loadings (15-20 %), masking the original acid-basic properties of the bulk material.

Thus, the aim of this work is to study the role of Co and Ni as reduced nanoparticles in the promotion of the steps catalyzed by these metals, but affecting, as little as possible, the acid-basic properties of the original bulk material (Mg-Al). We propose catalysts with only 1 wt. % of metal, prepared by surface deposition. This procedure is typically used with noble metals, but not so often for transition ones. In fact, in most of the works reported, the metal is introduced into the bulk structure, modifying the original coordination lattice by substituting the original cations [25,26]. The second modification proposed in this work is to feed controlled amounts of hydrogen, in order to both, keep reduced these nanoparticles, and to improve their performance in

hydrogenation steps. This idea is supported by our previous studies with Au/TiO_2 for this reaction, obtaining an improvement of 74 % in the conversion and almost 10 % in the 1-butanol selectivity when working in presence of H_2 [27].

2. Experimental Methods

2.1. Catalysts preparation

Mg-Al mixed oxide (Mg/Al = 3) was obtained by the calcination of the corresponding hydrotalcite, prepared by co-precipitation of the Mg and Al nitrates (Aldrich magnesium nitrate hexahydrate, and Aldrich aluminium nitrate nonahydrate) at low super-saturation and under sonication. The detailed procedure is reported in the literature [6]. The gel was precipitated by increasing the pH to 10 with a NaOH solution (10 wt. %) and it was aged at 353 K for 24 h. The solid phase was centrifuged, washed with deionized water to pH 7 and dried at 383 K for 24 h, yielding the hydrotalcite (HT). Finally, the mixed oxide was obtained by calcining the HT in flowing air, from 293 to 973 K with a temperature rate of 5 $K \cdot min^{-1}$, holding this set-point for 5 h.

The Ni/Mg-Al and Co/Mg-Al materials (1 wt. % of metal) were synthesized by incipient wetness impregnation, using nickel (II) nitrate 6-hydrate (Panreac), and cobalt (II) nitrate 6-hydrate (Panreac). After the impregnation, the catalysts were treated under airflow from 293 to 973 K with a temperature ramp of 5 $K \cdot min^{-1}$, holding this temperature for 5 h, in order to remove the precursor salts. The reduced metals were obtained by treating the materials in flowing H_2-Ar mixture (10 vol. % of H_2; 20 $mL \cdot min^{-1}$) at 823 K for 6 h, according to the results observed during the characterization of the calcined precursors. In order to avoid further metal re-oxidation, the reduction was performed in-situ before each experiment.

2.2. Catalysts characterization

Temperature-programmed reduction analyses (TPR) were carried out in a Micromeritics 2900 TPD/TPR instrument, in order to define the reduction temperature of the catalysts precursors. In good agreement with the typical procedure, 10 mg of calcined catalytic precursors were treated under H_2 flow (10 vol. % H_2/Ar) from 298 to 973 K, with a temperature rate of 2.5 K·min^{-1}. Once the final catalysts were obtained, morphologic properties were determined by N_2 physisorption at 77 K in a Micromeritics ASAP 2020 using the Brunauer-Emmett-Teller (BET) method to analyse the surface area, and the Barret-Joyner-Halenda (BJH) method to calculate the pore volume and diameter. Surface basicity and acidity were analysed by temperature programmed desorption (TPD) using a Micromeritics 2900 TPD/TPR. 10 mg were pre-treated in He flow and saturated with CO_2 or NH_3 to determine the basicity or acidity, respectively. The evolution of CO_2 and NH_3 signals were followed in a Pfeiffer Vacuum Omnistar Prisma mass spectrometer, as well as the temperature was increased at 2.5 K·min^{-1} between 298 and 973 K.

The crystallographic structure of the catalysts was determined by X-ray diffraction (XRD) using a Philips PW 1710 diffractometer with a CuKα line (1.54 Å) in the 2θ range within 5 and 80° at 2°·min^{-1} of scanning rate. High-resolution transmission electron microscopy (HRTEM) analyses of the fresh materials were carried out to determine the nanoparticle size and distribution, as well as the metal dispersion, in a JEOL JEM2100 instrument. H_2 chemisorption was also performed in order to determine the metal dispersion and the crystallite size of the fresh and used catalysts, using the same instrument as for the morphological study (Micromeritics ASAP 2020).

123 **2.3. Catalytic studies**

124 Activity experiments were carried out from 523 to 723 K (with steps of 50 K) in a
125 0.4 cm i.d. U-shaped fixed bed quartz reactor located inside a controlled electric
126 furnace. The catalyst (150 mg; 250-355 μm) was placed above a quartz wool plug. The
127 sample was pre-treated at 473 K for 1 hour in flowing He before each experiment.
128 Absolute ethanol was supplied with a syringe pump in the He or H_2-He (10 vol. % of H_2)
129 flow, causing the in situ vaporization, obtaining a 32 vol. % of ethanol, fed to the
130 reactor at 20 mL·min^{-1} (STP). These conditions were chosen according to the
131 optimization reported in our previous work and they correspond to a weight hourly
132 space velocity (WHSV) of 7.9 h^{-1} [20]. The outlet gases were on-line analysed with a
133 HP6890 Plus gas chromatograph with a flame ionization detector (GC-FID), using a
134 TRB-5MS capillary column. Additional GC-FID analyses were off-line performed
135 combining two columns (HP-Plot Q and HP-Plot MoleSieve 5A) in order to distinguish
136 and quantify ethylene and methane. Products identification was performed using
137 commercial standards and supported by GC-MS (Shimadzu QP-2010) by the same
138 methodology in the GC-FID. Operation conditions were selected in order to ensure that
139 the reported experiments are performed under kinetic regime, being mass transfer
140 effect negligible.

141 Conversions (x) were calculated from the ethanol concentrations at the reactor
142 inlet and outlet. Carbon balances were calculated by contrasting the total quantity of
143 carbon atoms at the reactor inlet and outlet, taking into account only the identified
144 products (compounds in Scheme 1). Yield was calculated by the following equation:

145 $$\eta_i(\%) = \left(\frac{\text{moles of ethanol fed converted to the product i}}{\text{moles of ethanol fed}}\right) \cdot 100 \qquad \text{Eq. 1}$$

146 The productivity of the different compounds (P_i) during the reaction (average
147 formation rate) were determined as follows:

148 $$P_i\ (mmol \cdot s^{-1} \cdot g_{cat}^{-1}) = \frac{F \cdot x \cdot \varphi_i}{W}$$ Eq. 2

149 F ≡ ethanol molar flow fed to the reactor (mmol·s^{-1})

150 W ≡ catalyst mass (g)

151 φ_i ≡ Selectivity for product i (moles of ethanol fed converted to a product i/ moles
152 of converted ethanol).

153 Diffuse reflectance infrared Fourier transform (DRIFT) spectroscopy experiments
154 were performed using a Thermo Nicolet Nexus FT-IR equipped with a Smart Collector
155 Accessory and a MCT/A detector. The material (20 mg) was placed inside the catalytic
156 chamber where the temperature was controlled. The sample was pre-treated at 473 K
157 for 1 h in He flow. Spectra were acquired in the 4000-650 cm^{-1} wavenumber range, after
158 subtraction of the KBr standard background. Spectra were recorded at same
159 temperatures as in the reactor allowing the comparison between both results, and
160 working under inert (He) or reducing conditions (10 vol. % H_2/He), as needed. Signals
161 were transformed to Kubelka-Munk units to obtain semi-quantitative results. This
162 method allows quantitatively analyze the amount of adsorbed species on the surface,
163 being the signal (for a same support and comparing analogous conditions) proportional
164 to the concentration of adsorbed species [28].

165

166 3. Results and discussion

167 3.1. Characterization of fresh catalysts

168 The morphological properties and surface chemistry of parent and metal-modified
169 materials have been analyzed by N_2 physisorption, CO_2-TPD and NH_3-TPD, being the main
170 results summarized in **Table 1**. No significant changes in surface area were observed, with only

171 the expected slight decrease after the metal deposition on the parent mixed oxide. In good
172 agreement, pore volume and diameter also slightly decrease. Metals mainly are deposited on
173 acid sites [29,30], being the strongest ones the most affected by the metal deposition. A very
174 similar behavior, disappearing more than 85 % of the initially present was observed in both
175 cases. As to the basicity, the decrease respect to the Mg-Al is less marked, being only relevant
176 in the case of the strongest sites. This phenomenon is more evident in the case of Ni material,
177 catalyst that only keeps the weak basic sites.

178 XRD analyses (**Figure S1**) corroborate that there are not significant changes in the general
179 structure of the bulk Mg-Al oxides, the same peaks for all the metal-modified catalysts being
180 observed. Periclase is the main phase in all the cases, with similar diffraction patterns for all
181 the catalysts. No signals related to the added metal species were detected, as expected
182 considering the low metal content. HRTEM analyses were carried out in order to determine
183 the metal particle size and dispersion. Representative histograms of crystallite sizes
184 distributions are depicted in **Figure 1** (corresponding micrographs are included in the
185 Supplementary Information, **Figure S2**); whereas crystallite sizes and metal dispersion data are
186 summarized in **Table 1**. A very high dispersion is observed (> 75 % in both the cases), with
187 nanoparticles around 1.3 nm large. These values are in good agreement with those reported in
188 the literature for similar catalysts prepared by this procedure [31].

189 The low crystallite sizes observed by HRTEM suggest a strong interaction between metal
190 and support. This hypothesis is congruent with the high reduction temperatures observed in
191 the TPR results (Figure 1c). According to the literature, the reduction of Ni nanoparticles takes
192 place at 640 K [32], whereas in our sample metal is mainly reduced at 698 K, with only a minor
193 shoulder at 640 K. The reaction from Co_3O_4 to Co is reported at $T \leq 623$ K when is supported
194 over alumina, and peaks around 773 K or above are associated with the reduction of Co-Al
195 mixed oxides [33]. Observing the TPR results obtained with the Co/Mg-Al material, two peaks

196 are highlighted at 565 and 750 K, which are related to the former and the latter reductions,
197 respectively.

198

199 ## 3.2. Reaction results under reducing atmosphere

200 The role of Co and Ni was studied by introducing hydrogen in the helium stream (10 vol. %
201 of H_2). In a previous blank experiment (without catalyst), ethanol conversions were negligible
202 at the temperature range considered in this article, so reported data are directly related to the
203 catalytic activity. The reducing conditions are expected to promote the hydrogenation steps of
204 the reaction mechanism, enhancing the 1-butanol yield, and to hinder oligomerization that
205 could strongly affect to the catalytic stability.

206 The evolution of the conversion, carbon mass balance and selectivity to the main
207 compounds with the reaction temperature is showed in **Figure 2** for the different tested
208 materials (Mg-Al, Co/Mg-Al and Ni/Mg-Al). Reactions with Mg-Al are also considered in order
209 to analyze any change in the basis mechanism because of the presence of H_2 in absence of any
210 metal. The evolution of other intermediates, obtained at lower but measurable
211 concentrations, is included in the Supplementary Data (**Table S1**). In all the cases, data
212 reported is the average results after three experiments, observing good reproducibility. The
213 decarbonylation of acetaldehyde, reaction catalyzed by several metals [34], is discarded in
214 these cases, since the highest yield to methane obtained was always lower than 0.2 % (value
215 observed with Co/Mg-Al at 723 K).

216 At the lowest temperatures, conversions obtained with and without metal are very
217 similar, these differences increasing as temperature increases. Thus, conversions of 54.6 (Ni)
218 and 56.3 % (Co) are obtained at 723 K, corresponding to relative increments higher than 25 %
219 in comparison to those obtained with the Mg-Al (43.1 % at 723 K). These results indicate that

metal nanoparticles play a relevant role at reducing conditions. Concerning to the carbon balance, values higher than 80 % were obtained for Ni and Co materials at temperatures lower than 700 K, whereas at 723 K they decrease to close to 70 %. At same conditions, the value reached with Mg-Al was 76.2 %. These slight differences are related to the lower activity observed with the bulk material, being the production of higher alcohols (>C4) at highest temperatures the main reason of the decrease with the metal modified ones. These compounds were detected by the GC, but their low individual amount prevents its exact quantification. However, the better carbon balance closures obtained with the metal modified materials at temperatures lower than 700 K suggest a higher global selectivity to the main reaction pathway.

Regarding the selectivity to different reaction products, a positive effect of reducing conditions is clearly observed by comparing the lower selectivity to acetaldehyde obtained with both, Ni and Co materials (in contrast to the parent mixed oxide, at all the temperatures tested); and the higher selectivities obtained for 1-butanol (Fig. 2b). In fact, 1-butanol selectivity reaches maximum values close to 33 % with Co and Ni, whereas the maximum selectivity obtained for the bulk material is lower than 23 % (results at 623 K for all the materials). These results are considerably higher than other previously published working with Co in larger amounts (higher than 10 %) and higher pressures (8 % butanol selectivity at 513 K and 70 bar) [21], highlighting the better behavior of these metals as nanoparticles instead of as cations.

A theoretical study about the equilibria conditions was carried out to guarantee that equilibria is not conditioning the values obtained. According to Moteki and Flaherty [9], the main mechanism is divided into 14 individual steps (considering both, adsorption and reaction processes), being most of them equilibria steps. According to this proposal, the acetaldehyde productivity could be theoretically conditioned by the ethanol adsorption, the proton

abstractions to obtain the ethoxyde and acetaldehyde on the catalytic surface, and their corresponding adsorption-desorption equilibria. Despite the complexity of the analysis of these individual steps, a first approach supposes the acetaldehyde formation as an equilibrium step considering the ethanol and hydrogen in the medium. Thus, experimental results were used to estimate the reaction quotients (Q) and these values were compared to the theoretical equilibrium constant K, obtaining, in the worst case, a Q/K ratio lower than 0.002, suggesting that the reaction is far from equilibrium at these conditions.

Despite the metal used, the general profiles are similar, with a decreasing trend of acetaldehyde, typical evolution of a primary product; and a formation pattern characterized by a maximum and a subsequent decrease for the 1-butanol, that responds to a product obtained after serial steps of a global reaction that continues and produces undesired compounds (if temperature conditions are too severe). One of the main side-products is the ethylene, with a continuous increasing trend, more marked in the case of the bulk material. Consequently, no evidences of any change in the main reaction mechanisms were observed when introducing metals or reducing conditions, allowing the analysis of the influence of metals and reducing conditions.

3.3. Analyses of reactions results

Considering that the aim of this work is to enhance the 1-butanol productivity, the good results shown in Fig. 2 can be better illustrated analyzing the influence of metals and reducing conditions on the 1-butanol productivity. Since medium strength basic sites are considered the most active sites for aldol condensation, **Figure 3** shows the 1-butanol productivity under reducing conditions, normalized by the concentration of medium strength basic sites, according the expression of the α parameter, defined as follows:

$$\alpha = \frac{\left(\frac{[\text{butanol productivity}]}{[\text{surface basicity}]_{\text{medium strength}}}\right)_{\text{metal/Mg–Al}}}{\left(\frac{[\text{butanol productivity}]}{[\text{surface basicity}]_{\text{medium strength}}}\right)_{\text{Mg–Al}}} \quad \text{Eq. 3}$$

A clear improvement is observed; mainly at the mildest conditions, which is an extra advantage of this strategy. At the lowest temperature, the α parameter is almost 6 times higher with both metal modified materials than the corresponding one with the Mg-Al, being almost constant with the Co when temperature increases to 573 K. As the temperature increases, the goodness of this configuration decreases, but the productivity is still higher at the highest temperature. These results suggest that the differences between parent and metal-promoted oxides cannot be explained only in terms of their reactivity for aldol condensation (despite this reaction is often considered as the rate-determining step [9,15]). Thus, the role of the catalyst properties on dehydrogenations and hydrogenations must be considered in detail.

In order to get a better understanding on these reactions, strongly dependent on hydrogen concentration, the same set of experiments was performed in absence of hydrogen, being the results depicted in **Figure 4**. First step affected by the metal presence is the ethanol dehydrogenation. The global effect of reducing conditions and metal catalyst in this reaction is compared in **Figure 5**. For this analysis, AA corresponds to acetaldehyde whereas the term "C4 main route" involves the sum of the yields to crotonaldehyde, crotyl alcohol, butanal, 1-butanol, 1,3-butadiene and ethyl acetate, in order to have an idea of the overall catalytic performance for the ethanol dehydrogenation. A clear increasing trend is obtained in all cases, but significant differences, as function of the materials, are observed when comparing the effect of inert or reducing atmosphere. When working under inert conditions, best results are obtained using the parent Mg-Al (almost 3 times higher comparing to the bifunctional ones). It should be highlighted the unexpected effect of reducing conditions when Mg-Al is used as catatalyst, the presence of hydrogen hindering the reaction. Considering that there is not any

metal phase to activate the hydrogen molecule, a similar behavior would be expected. However, there are clear differences that must be directly related to adsorption processes, suggesting a non-dissociative adsorption of hydrogen molecules on the catalytic surface, hindering the ethanol adsorption needed for the aldolization step. This hypothesis is supported by previous works that noticing the H_2 adsorption on acidic sites (OH groups) using similar oxides [35,36]. Trends achieved with the bifunctional materials show higher slope than those observed for the parent Mg-Al. This fact happens since dehydration side reactions are more favored at increasing temperatures, being more relevant when using the bulk Mg-Al because of its higher acidity (supported by Table 1, and Fig. 2c and 4c) [35].

Concerning to the comparison between bifunctional materials, the nickel catalyst reaches the lowest values and its trend shows lower slope than that observed with the cobalt one. This is in agreement with the low concentration and strength of basic sites owned by the Ni/Mg-Al, together with the preference of this metal for favoring hydrogenations [37]. In presence of hydrogen, the Co/Mg-Al catalyst shows the best dehydrogenation performance, reaching improvements up to of 22 and 87 % in regard to the Ni/Mg-Al and Mg-Al materials. Thus, it is confirmed that hydrogen supplying enhances the performance to the main route preceded by ethanol dehydrogenation. This net improvement under reducing atmosphere is explained by the effect of the subsequent steps. It can be supposed that cobalt enhances the consumption of acetaldehyde to produce the C4 compounds, displacing the equilibrium to the formation of more acetaldehyde. In order to check this hypothesis, the following steps must be analyzed.

Figure 6 illustrates the relative weight of condensation steps, analyzing the aldol condensation (Fig. 6a) and the acetaldehyde transformation into ethyl acetate via Tishchenko-type reaction (Fig. 6b). The highest condensation activity was obtained with Ni/Mg-Al under reducing conditions, with similar values as those obtained with Mg-Al under inert atmosphere. Ni/Mg-Al shows higher aldolization capacity than the expected one,

318 considering the low concentration of basic sites of this material. This analysis suggests that the
319 main role of Ni is to improve the subsequent steps that consume the condensation adduct,
320 shifting the equilibrium. This fact is congruent with the larger improvement observed in
321 presence of hydrogen, relating the profile with the following hydrogenation steps. The
322 different behavior of the Co material must be highlighted. With this material, a strong
323 influence of atmosphere is observed, enhancing the ethyl acetate in presence of hydrogen.
324 Both compounds, ethyl acetate and crotonaldehyde, are obtained from ethanol, but involving
325 different intermediates: acyl for the ethyl acetate (CH_3-C*=O*) and enolate (CH_2*-CH=O) [38].
326 Results obtained suggest that the presence of hydrogen and cobalt inhibits to some degree the
327 formation of the enolate intermediate from acetaldehyde ($^{\beta}$C-H scission hindered by hydrogen
328 adatoms), enhancing the selectivity to the esterification pathway, mainly at low temperatures.
329 This is the reason explains the poor aldolization results despite the higher acetaldehyde
330 formation rate with Co-containing material, the most active for dehydrogenation activity.

331 The study of hydrogenation step is shown in **Figure 7**, analyzing the ratio between the
332 1-butanol selectivity and the selectivity for all the C4 condensation adducts. The different role
333 of each metal is clearly observed in this plot. Ni/Mg-Al catalyst shows the highest adducts
334 hydrogenation activity, mainly under reductive atmosphere, being this positive effect less
335 evident as the temperature increases. On the other hand, the absence of any metal phase
336 limits the hydrogenation activity of Mg-Al and, as a consequence, hydrogen has not any
337 positive effect when this material is used. Concerning to the Co catalysts, they do not show any
338 noticeable hydrogenation activity, being the obtained results similar or even worse than the
339 corresponding to the parent mixed oxide. The decreasing trend observed in almost all the
340 cases at the highest temperatures is caused by the higher relevance of oligomerization
341 reactions (in good agreement with the observed decrease in the carbon mass balance) and
342 also dehydration to produce 1,3-butadiene at the most severe conditions.

In order to verify all these hypothesis, DRIFT spectroscopy experiments were carried out, trying to identify relevant differences in the adsorption modes of the compounds involved in the reaction as function of the material and atmosphere conditions. DRIFT analyses were carried out at similar conditions as in the reaction medium, being possible the direct comparison of both results. As examples of the most significant results, spectra obtained at 573 K and 723 K are compared in **Figure 8**, under inert and reducing conditions.

The same three regions, related to specific functional groups, were observed for all the materials, corroborating that same type of interactions are taken place. The first one is identified as the stretching mode of CO (1050 cm^{-1}) [20], being related to the adsorption of alkoxide species. The second one, at 1580 cm^{-1} corresponds to the stretching vibration mode of C=C bonds (unsaturated alcohols and aldehydes), such as the crotonaldehyde and crotyl alcohol [20]. Under inert atmosphere, highest intensities of these adsorption modes are in good agreement with the highest concentration of acid sites (almost six times higher with Mg-Al than with the bifunctional ones, **Table 1**), mainly at 723 K. Consequently, aldehydes and alcohols present in the reaction media, mainly the heaviest ones, are adsorbed time enough to promote subsequent reactions yielding heavier compounds [39]. The high decrease of these signals when working under reducing conditions suggest that hydrogen hinders the adsorption of these compounds, avoiding their further reactions. The third band, at 1740 cm^{-1}, is related to the stretching vibration mode of C=O of aldehydes [20]. This band is only observed with Mg-Al at 723 K under inert conditions, suggesting the presence of relevant amount of crotonaldehyde adsorbed on the catalytic surface. There are other two bands clearly observed, at 950 and 1440 cm^{-1}, approximately. These bands correspond to common vibration modes of CH_3 (rocking and deforming one, respectively) [20], so they are not useful to identify any relevant molecule.

If results under inert and reducing conditions are compared, there is a clear difference between Mg-Al and the metal-modified materials, mainly Ni. Spectra obtained with the parent material are almost the same, in good agreement with the negligible role of hydrogen in absence of any metal phase. On the contrary, signals generally decrease for the metal-modified catalysts, suggesting that adsorption is less relevant because of the presence of hydrogen and the lower concentration of strong basic and acid sites. Most relevant results are obtained with Ni/Mg-Al under reducing conditions, with almost null interactions related to heavy compounds. This fact corroborates the direct link between hydrogenation activity and hindering permanent adsorption and the consequent oligomerization.

3.4. **Overall effect on the 1-butanol productivity**

In order to determine the optimal combination of catalyst and reaction conditions for maximize 1-butanol production, **Figure 9** summarizes the 1-butanol productivity. Data shown correspond to an analysis of the different productivity rates, normalizing all the values by the corresponding ones for the bulk material (β), at inert or reducing conditions, defined as:

$$\beta = \frac{[P_{1-butanol}]_{metal/Mg-Al}}{[P_{1-butanol}]_{Mg-Al}} \qquad \text{Eq. 4}$$

In global terms, the influence of metals is more relevant at low temperatures, being their effect almost negligible over 673 K. This is also an advantage of this procedure, increasing the green character of this process, obtaining good results at milder conditions than the normally used in the literature [8,11]. At low temperatures, the reducing atmosphere also plays a key role, obtaining relative rates more than six times higher than the obtained under inert atmosphere (in both cases). The highest 1-butanol productivity is reached at 573 K with the Co, with eight rates eight times higher than the one obtained with Mg-Al. Thus, the need of reducing conditions is also justified, observing clear improvements at temperatures too low to

produce the hydrogenations by MPV and surface mediated hydrogen-atom transfer mechanisms.

4. Conclusions

According to the deep analysis of the ethanol gas-phase condensation, the highest complexity of this mechanism is remarked. As consequence, it is very difficult to determine an optimum material with good properties for all the individual steps. Cobalt highlights by its high dehydrogenation capacity but it also enhances the ethyl acetate production (undesired side reaction). On the other hand, Nickel presents a relevant activity in aldol condensation and a high activity of the C=O and C=C hydrogenation, obtaining the best results for these two stages. In this case, a positive role of hydrogen is clearly observed. Nickel also limits the oligomerization (undesired reaction), as it was observed by DRIFT spectroscopy. Bands related to the adsorption of higher alkoxides are much more relevant with this material, mainly under inert atmosphere.

Thus, the 1-butanol productivity (target compound) is conditioned by the balance of all these stages. Under the conditions tested in this work, the dehydrogenation step controls the final result, obtaining the highest amount of 1-butanol when Co/Mg-Al is used, mainly at low temperature. At these mild conditions, when this reaction prevails over the dehydration and despite the higher amount of ethyl acetate obtained with this material. This improvement is much more relevant under reducing conditions, highlighting also the role of hydrogenation steps. On the other hand, results obtained with Ni/Mg-Al are also relevant, obtaining good productivity of 1-butanol and increasing the global selectivity to the main process (less amount of ethylene, ethyl acetate and oligomers).

Acknowledgments

The authors acknowledge financial support from the Ministry of Economy and Competitiveness of the Government of Spain (Contract: CTQ2014-52956-C3-1-R). Jorge Quesada also thanks for his Ph.D. fellowship (PA-14-PF-BP14-105) of the Severo Ochoa Program of the local Government of the Principality of Asturias.

References

[1] L. Faba, E. Díaz, S. Ordóñez, Renew. Sust. Energ. Rev. 51 (2015) 273-287.

[2] W.E. Taifan, G.X. Yan, J. Baltrusaitis, Catal. Sci. Technol. 20 (2017) 4648-4668.

[3] J.H. Earley, R.A. Bourne, M.J. Watson, M. Poliakoff, Green Chem. 17 (2015) 3018-3025.

[4] S. Hanspal, Z.D. Young, H. Shou, R.J. Davis, ACS Catal. 5 (2015) 1737-1746.

[5] L. Silvester, J.F. Lamonier, J. Faye, M. Capron, R.N. Vannier, C. Lamonier, J.L. Dubois, J.L. Couturier, C. Calais, F. Dumeignil, Catal. Sci. Technol. 5 (2015) 2994-3006.

[6] S. Ordóñez, E. Díaz, M. León, L. Faba, Catal. Today 167 (2011) 71-76.

[7] J.T. Koslowski, R.J. Davis, J. Energy Chem. 22 (2013) 58-64.

[8] S. Ogo, A. Onda, K. Iwasa, A. Fukuoka, J. Yanigisawa, J. Catal. 296 (2012) 24-30.

[9] T. Moteki, D.W. Flaherty, ACS Catal. 6 (2016) 4170-4183.

[10] A. S. Ndou, N. Plint, N.J. Coville, Appl. Catal. A 251 (2003) 337-345.

[11] T. Tshuchida, J. Kubo, T. Yoshioka, S. Sakuma, T. Takeguchi, W. Ueda, J. Catal. 259 (2008) 183-189.

[12] C.R. Ho, S. Shylesh, A.T. Bell, ACS Catal. 6 (2016) 939-948.

[13] J.I. Di Cosimo, V.K. Díez, M. Xu, E. Iglesia, C.R. Apesteguía, J. Catal. 178 (1998) 499-510.

[14] K.A. Goulas, G. Gunbas, P.J. Dietrich, S. Sreekumar, A. Grippo, J.P. Chen, A.A. Gokhale, F.D. Toste, ChemCatChem 9 (2017) 1-10.

[15] J.T. Kozlowski, R. J. Davis, ACS Catal. 3 (2013) 1588-1600.

[16] J. Zaffran, C. Michel, F. Delbecq, P. Sautet, J. Phys. Chem. C 119 (2015) 12988-12998.

[17] M.A. Ortuño, V. Bernales, L. Gagliardi, C. J. Cramer, J. Phys. Chem. C 120 (2016) 24697-24705.

[18] J.J. Ramos, V.K. Díez, C.A. Ferretti, P.A. Torresi, C.R. Apesteguía, J.I. Di Cosimo, Catal. Today 172 (2011) 41-47.

[19] J.I. Di Cosimo, A. Acosta, C.R. Apesteguía, J. Mol. Catal. A 222 (2004) 87-96.

[20] J. Quesada, L. Faba, E. Díaz, S. Ordóñez, Appl. Catal. A 542 (2017) 271-281.

[21] T. Riittonen, K. Eränen, P. Mäki-Arvela, A. Shchukarev, A.R. Rautio, K. Kordas, N. Kumar, T. Salmi, J.P. Mikkola, Renew. Energ. 74 (2015) 369-378.

[22] J.J. Bravo-Suárez, B. Subramaniam, R.V. Chaudhari, Appl. Catal. A 455 (2013) 234-246.

[23] J. Pang, M. Zheng, L. He, L. Li, X. Pan, A. Wang, X. Wang, T. Zhang, J. Catal. 344 (2016) 184-193.

[24] X. Wu, G. Fang, Z. Liang, W. Leng, K. Xy, D. Jiang, J. Ni, X. Li, Catal. Commun. 100 (2017) 15-18.

[25] I.C. Marcu, N. Tanchoux, F. Fajula, D. Tichit, Catal. Lett. 143 (2013) 23-30.

[26] M. León, E. Díaz, A. Vega, S. Ordóñez, A. Auroux, Appl. Catal. B 102 (2011) 590-599.

[27] J. Quesada, R. Arreola-Sánchez, L. Faba, E. Díaz, V.M. Rentería-Tapia, S. Ordóñez, Appl. Catal. A 551 (2018) 23-33.

[28] J. Sirita, S. Phanichphant, F.C. Meunier, Anal. Chem. 79 (2007) 3912-3918.

[29] P. Burattin, M. Che, C. Louis, J. Phys. Chem. B 102 (1998) 2722-2732.

[30] I. Obregón, I. Gandarias, A. Ocio, I. García-García, N. Álvarez de Eulate, P.L. Airas, Appl. Catal. B 210 (2017) 328-341.

[31] K. L. Luska, P. Miglowski, S. E. Sayed, W. Leitner, ACS Sustain. Chem. Eng. 4 (2016) 6186-6192.

[32] A. Parmaliana, F. Arena, F. Frusteri, N. Giordano, J. Chem. Soc. Faraday Trans. 86 (1990) 2663-2669.

[33] O.O. James, D. Maity, J. Pet. Technol. Altern. Fuels 7 (2016) 1-12.

[34] E.I. Gürbüz, D. Hibbitts, E. Iglesia, J. Am. Chem. Soc. 137 (2015) 11984-11995.

[35] H.U. Blaser, A. Schnyder, H. Steiner, F. Rössler, P. Baumeister, Handbook of Heterogeneous Catalysis, 2nd ed., Editors: G. Ertl, H. Knözinger, F. Schüth, J. Weitkamp, Wiley-VCH, Weinheim, 2008, Vol. 7, p. 3286.

473 [36] J.I. Di Cosimo, C.R. Apesteguía, M.J.L. Ginés, E. Iglesia, J. Catal. 190 (2000) 261-275.

474 [37] D.D. Eley, M.A. Zammit, J. Catal. 21 (1971) 377-383.

475 [38] M.E. Sad, N. Neurock, E. Iglesia, J. Am. Chem. Soc. 133 (2011) 20384-20398.

476 [39] D. Leckel, Energ. Fuel 21 (2007) 662-667.

SCHEME CAPTION

Scheme 1. Reaction mechanism for the gas phase ethanol upgrading [5-8]. Symbols: (A) ethanol; (B) acetaldehyde; (C) crotonaldehyde; (D) crotyl alcohol; (E) butanal; (F) 1-butanol; (G) 1,3-butadiene; (H) ethylene; (I) diethyl ether; (J) ethyl acetate.

FIGURE CAPTION

Figure 1. (a) HRTEM histograms of crystallite diameter of Ni/MgAl (100 particles); (b) HRTEM histograms of Co/MgAl (100 particles); (c) TPR results obtained for Ni/Mg-Al and Co/Mg-Al materials

Figure 2. Catalyst performance at different temperatures under reductive conditions as function of the temperature for the reaction catalyzed by (●) Mg-Al*; (▲) Ni/Mg-Al; and (■) Co/Mg-Al. Results in terms of: (a) conversion (black) and carbon balance (white); (b) acetaldehyde (black) and butanol (white) selectivity; (c) ethylene (black) and 1,3-butadiene (white) selectivity. *Results taken from a previous work [20].

Figure 3. Comparison of the relative 1-butanol concentration obtained under reducing conditions. Results normalized by the Mg-Al ones. Values correspond to 523 K (white); 573 K (light grey); 623 K (dark grey); 673 K (black) and 723 K (bars)

Figure 4. Catalyst performance at different temperatures under inert conditions as function of the temperature for the reaction catalyzed by (●) Mg-Al; (▲) Ni/Mg-Al; and (■) Co/Mg-Al. Results in terms of: (a) conversion (black) and carbon balance (white); (b) acetaldehyde (black) and butanol (white) selectivity; (c) ethylene (black) and 1,3-butadiene (white) selectivity.

Figure 5. Analysis of the dehydrogenation capacity as function of the catalyst and reaction temperature. Results under inert (open symbols) and reducing atmosphere (solid symbols). Symbol: Mg-Al (●); Co/Mg-Al (■); Ni/Mg-Al (▲)

Figure 6. Analysis of (a) aldol condensation step and (b) acetaldehyde esterification side-reaction, under inert (white) and reducing (black) conditions. *See Figure 5 for symbols*

Figure 7. Analysis of selective hydrogenation to 1-butanol under inert (white) and reducing (black) conditions. *See Figure 5 for symbols*

Figure 8. DRIFT spectra of different catalyst during the ethanol condensation under inert (lines) or reducing conditions (broken lines). Results corresponding to reaction at (a) 573 K and (b) 723 K. *Relative intensities of (b) spectra are ten times higher than those observed in the (a) spectra*

Figure 9. Comparison of the relative 1-butanol production rate obtained with the different materials under inert (bars) and reducing atmosphere (solid colors). Data normalized as function of results with the bulk MgAl. Values corresponding to Ni (grey) and Co (black) materials

TABLE CAPTION

Table 1. Main results of the fresh catalysts characterization: morphological properties, density and distribution of the acid and basic sites, and HRTEM results. *Results taken from a previous work [20].

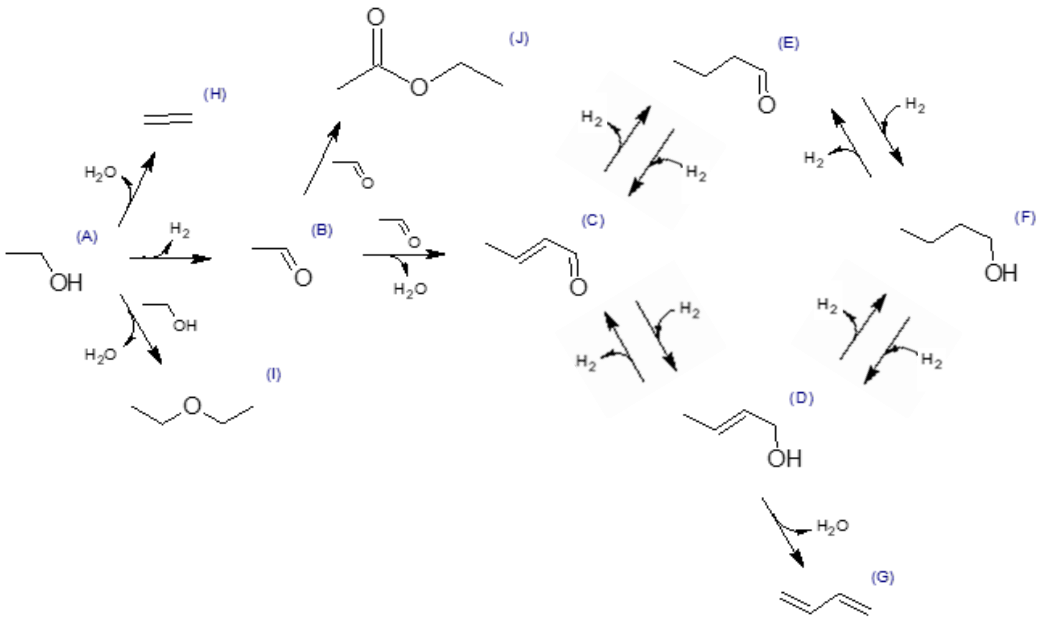

519

520 **Scheme 1.** Reaction mechanism for the gas phase ethanol upgrading [5-8]. Symbols: (A)

521 ethanol; (B) acetaldehyde; (C) crotonaldehyde; (D) crotyl alcohol; (E) butanal; (F) 1-butanol; (G)

522 1,3-butadiene; (H) ethylene; (I) diethyl ether; (J) ethyl acetate.

523

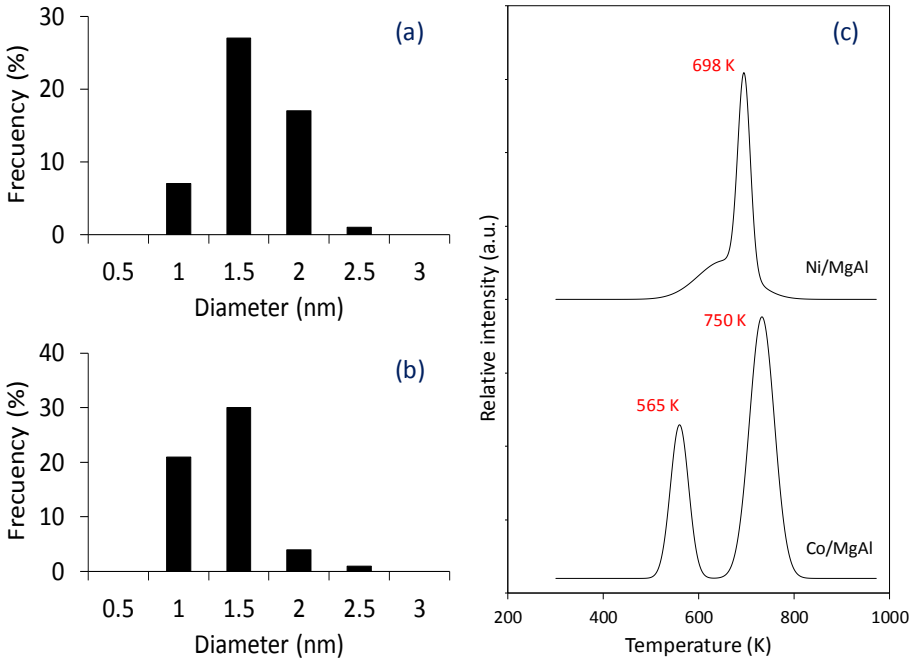

524

525 **Figure 1.** (a) HRTEM histograms of crystallite diameter of Ni/MgAl (100 particles); (b) HRTEM

526 histograms of Co/MgAl (100 particles); (c) TPR results obtained for Ni/Mg-Al and Co/Mg-Al

527 materials

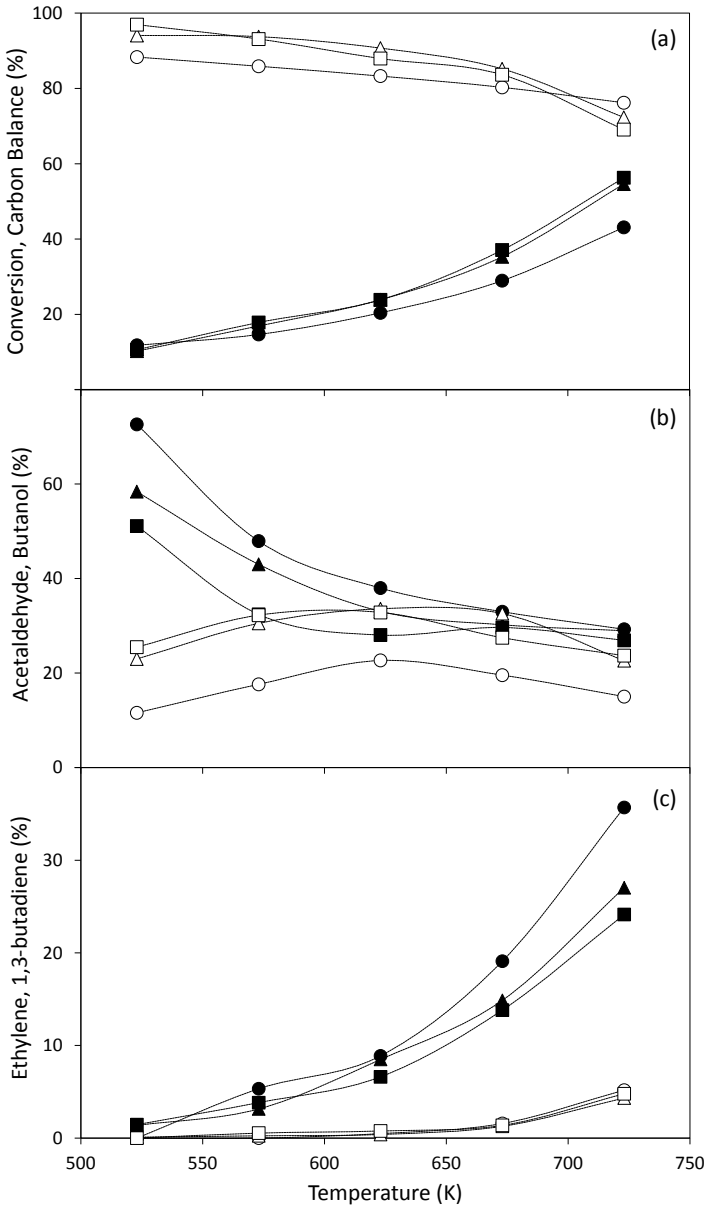

Figure 2. Catalyst performance at different temperatures under reductive conditions as function of the temperature for the reaction catalyzed by (●) Mg-Al*; (▲) Ni/Mg-Al; and (■) Co/Mg-Al. Results in terms of: (a) conversion (black) and carbon balance (white); (b) acetaldehyde (black) and butanol (white) selectivity; (c) ethylene (black) and 1,3-butadiene (white) selectivity. *Results taken from a previous work [20].

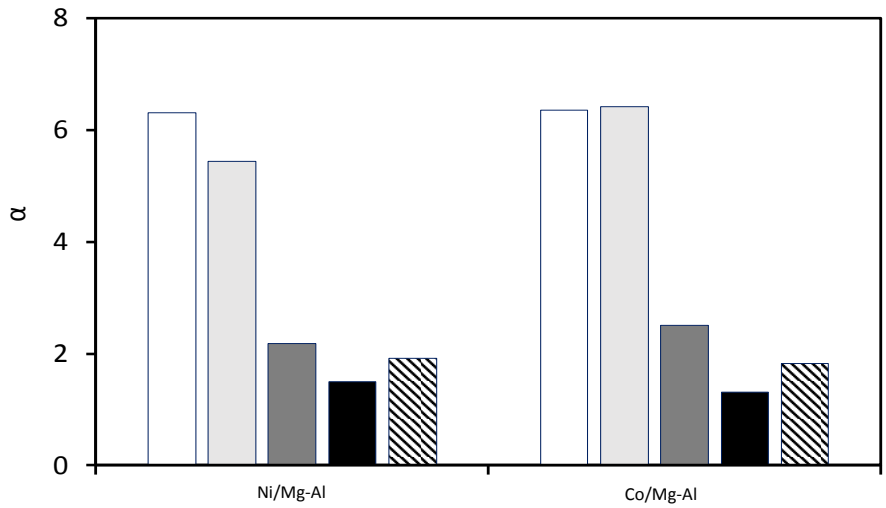

536

537 **Figure 3.** Comparison of the relative 1-butanol concentration obtained under reducing
538 conditions. Results normalized by the Mg-Al ones. Values correspond to 523 K (white); 573 K
539 (light grey); 623 K (dark grey); 673 K (black) and 723 K (bars)

540

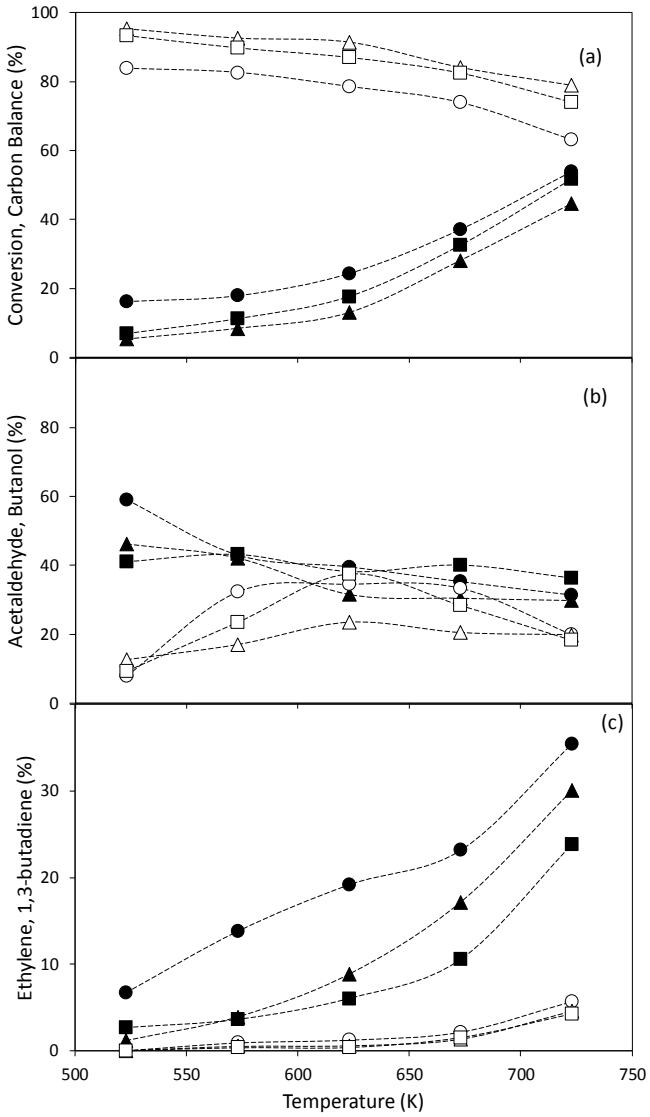

541

542

543 **Figure 4.** Catalyst performance at different temperatures under inert conditions as function of

544 the temperature for the reaction catalyzed by (●) Mg-Al; (▲) Ni/Mg-Al; and (■) Co/Mg-Al.

545 Results in terms of: (a) conversion (black) and carbon balance (white); (b) acetaldehyde (black)

546 and butanol (white) selectivity; (c) ethylene (black) and 1,3-butadiene (white) selectivity.

547

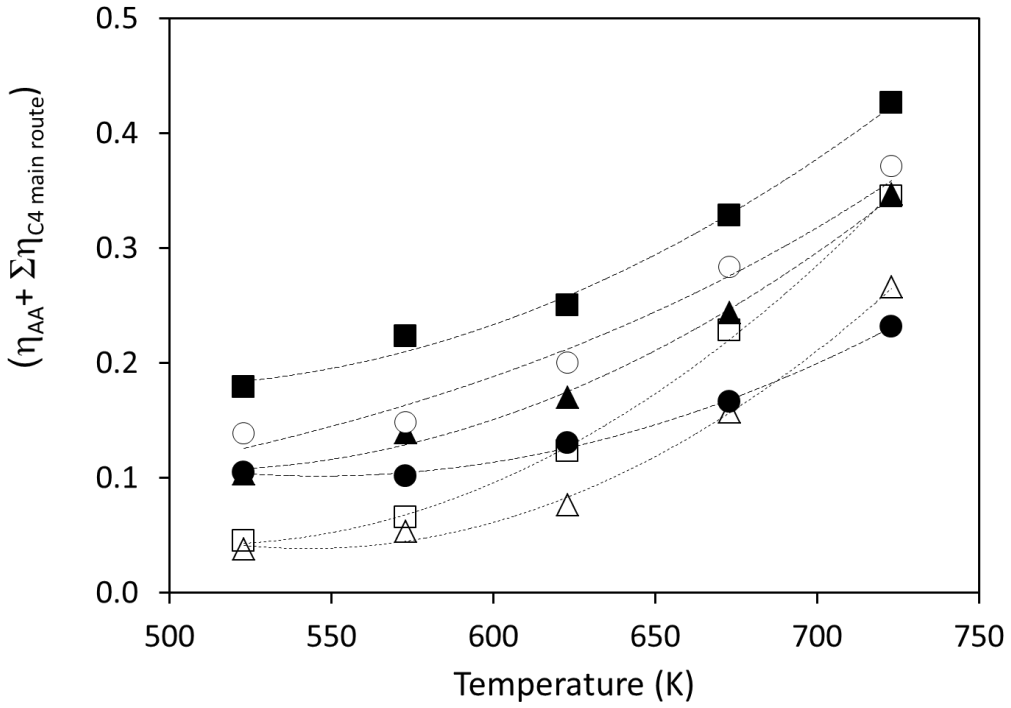

548

549 **Figure 5.** Analysis of the dehydrogenation capacity as function of the catalyst and reaction

550 temperature. Results under inert (open symbols) and reducing atmosphere (solid symbols).

551 Symbol: Mg-Al (●); Co/Mg-Al (■); Ni/Mg-Al (▲)

552

553

554

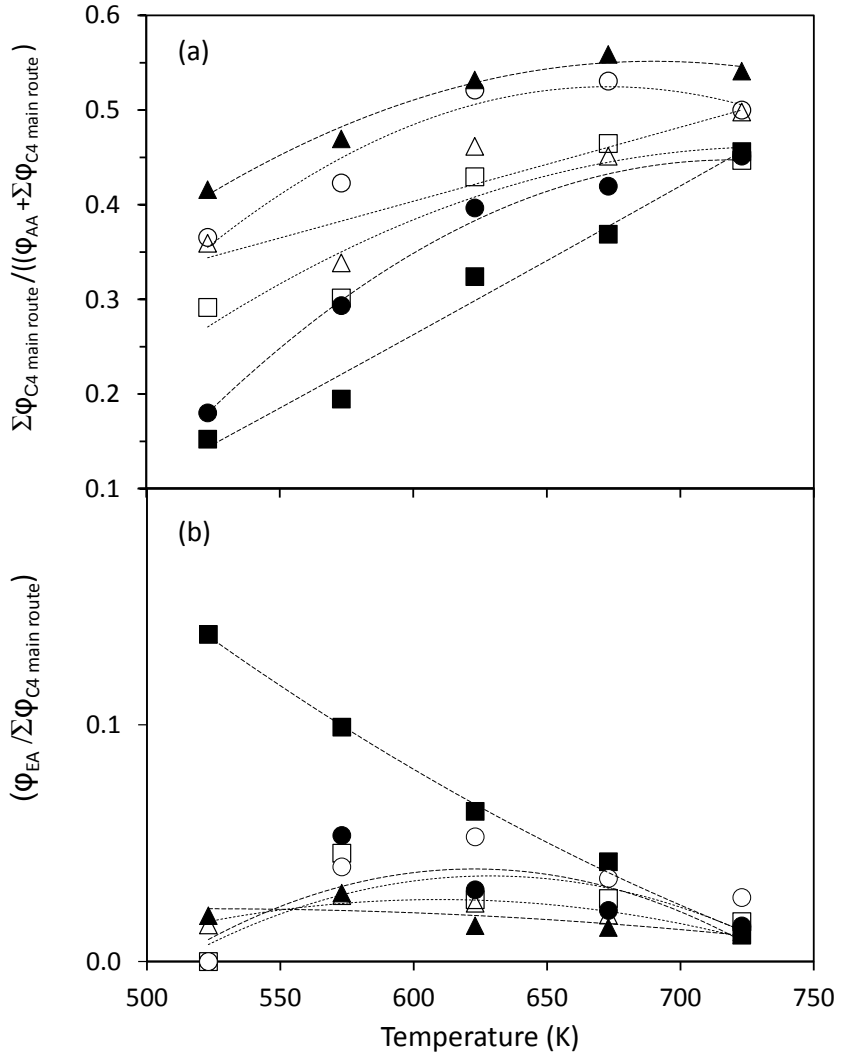

Figure 6. Analysis of (a) aldol condensation step and (b) acetaldehyde esterification side-reaction, under inert (white) and reducing (black) conditions. *See Figure 5 for symbols*

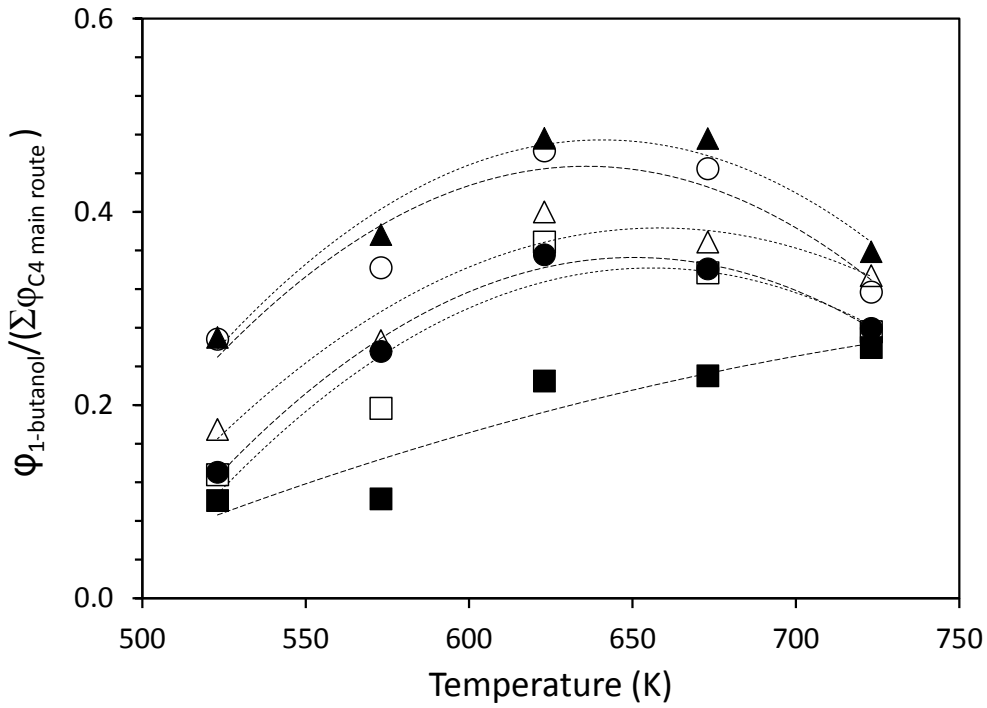

Figure 7. Analysis of selective hydrogenation to 1-butanol under inert (white) and reducing (black) conditions. *See Figure 5 for symbols*

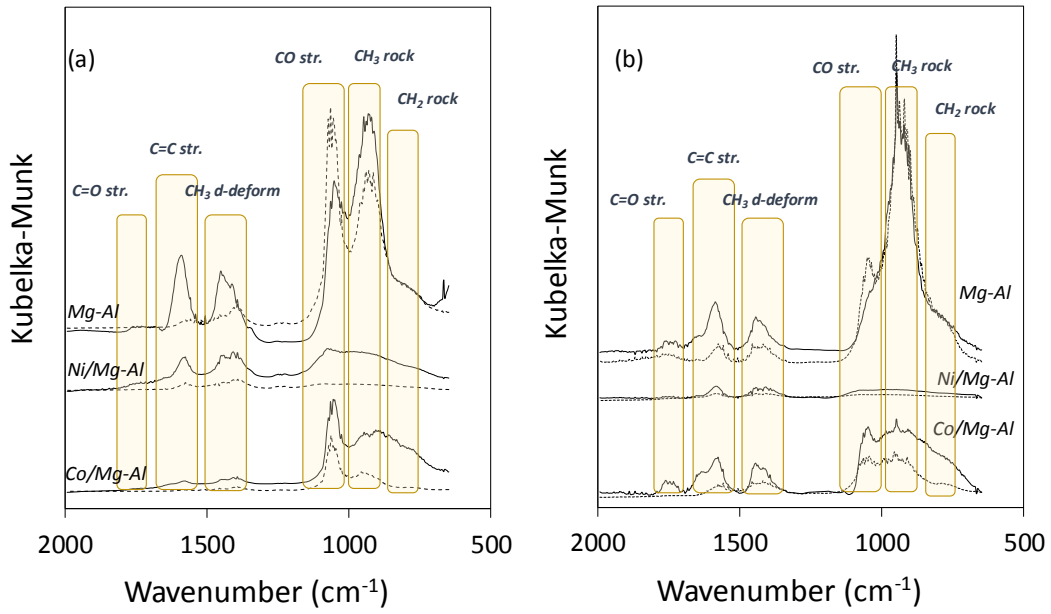

565

566 **Figure 8.** DRIFT spectra of different catalyst during the ethanol condensation under inert (lines)

567 or reducing conditions (broken lines). Results corresponding to reaction at (a) 573 K and (b)

568 723 K. *Relative intensities of (b) spectra are ten times higher than those observed in the (a)*

569 *spectra*

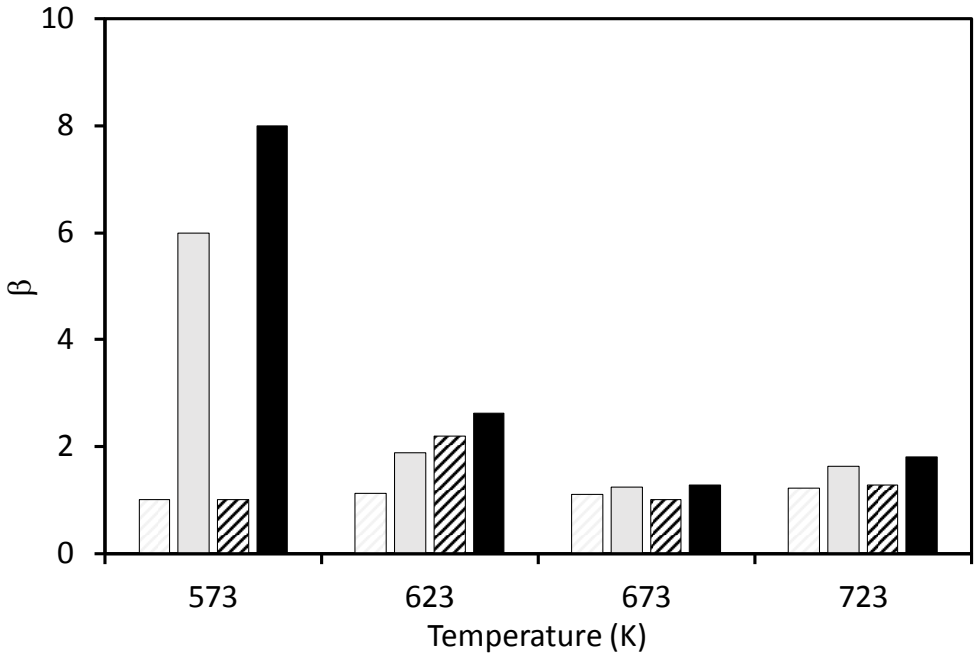

Figure 9. Comparison of the relative 1-butanol production rate obtained with the different materials under inert (bars) and reducing atmosphere (solid colors). Data normalized as function of results with the bulk MgAl. Values corresponding to Ni (grey) and Co (black) materials

Table 1. Main results of the fresh catalysts characterization: morphological properties, density and distribution of the acid and basic sites, and HRTEM results. *Results taken from a previous work [20].

Catalyst	Morphological properties			Acid sites (µmol g^{-1}), [T (K)]			Basic sites (µmol g^{-1}), [T (K)]			HRTEM	
	S (m^2 g^{-1})	D_p (Å)	V_p (cm^3 g^{-1})	weak	medium	strong	weak	medium	strong	Metal dispersion (%)	Crystallite diameter (nm)
Mg-Al*	226	135	0.7	11.3 [345, 370]	12.5 [450]	41.8 [630, 800]	49.7 [340]	71.7 [400]	238.6 [630, 670, 800]	-	-
Ni	182	59	0.4	3.9 [329, 365]	3.3 [419]	4.0 [517]	55.8 [328, 377]	10.6 [430]	-	78.6	1.3
Co	207	60	0.4	2.9 [325, 358]	3.1 [408]	5.4 [508]	51.0 [355]	70.2 [415, 491]	53.8 [607, 738]	78.7	1.3